Quantitative Imaging in Whole-mount Zebrafish Embryos Traces Morphogen Gradient Maintenance and Noise Propagation in BMP Signaling

Xu Wang (wang_xu2020@grmh-gdl.cn)
Guangzhou Regenerative Medicine and Health Guangdong Laboratory
Linlin Li
Purdue University West Lafayette
Ye Bu
Purdue University West Lafayette
Yixuan Liu
Purdue University West Lafayette
Tzu-Ching Wu
Purdue University West Lafayette
David M. Umulis
Purdue University West Lafayette

Research Article

Keywords: Dorsoventral (DV), BMP, zebrafish gastrula, DV patterning, gradient shaping

Posted Date: December 14th, 2021

DOI: https://doi.org/10.21203/rs.3.rs-1122294/v1

Abstract

Dorsoventral (DV) embryonic patterning relies on precisely controlled interpretation of morphogen signaling. In all vertebrates, DV axis specification is informed by gradients of bone morphogenetic proteins (BMPs). We developed a 3D single-molecule mRNA quantification method in whole-mount zebrafish to quantify the inputs and outputs in this pathway. In combination with 3D computational modeling of zebrafish embryo development, data from this method revealed that sizzled (Szl), shaped by BMP and Nodal signaling, maintained a consistent inhibition level with chordin (Chd) to maintain the BMP morphogen gradient. Intriguingly, intrinsic BMP morphogen expression is highly noisy at the ventral marginal layer in the early zebrafish gastrula, where the gradient for DV patterning is established, which implies an unexpected role for noise in gradient shaping.

Introduction

During embryonic development, morphogen gradients contribute to positional information for each cell and drive individual cell fate determination; moreover, stochastic noise can toggle gene expression levels (Hasty et al., 2000) and facilitate gene expression boundaries (Zhang et al., 2012). BMP ligands signal by binding to BMP receptors that form a higher-order receptor complex that phosphorylates the Smad5 transcription factor that binds to a co-Smad bef. BMP acts as a morphogen in numerous developmental contexts, including the patterning of the embryonic dorsal/ventral axis, neural tube, and Drosophila wing disc (Tuazon et al. 2020)(Bier and De Robertis 2015)(Briscoe and Small 2015). Szl, a downstream product of pSmad-mediated BMP signaling, also acts to regulate BMP signaling. Szl competitively binds proteinases (Tolloid and Bmp1) that target Chordin, an inhibitor of BMP signaling (Tuazon et al. 2020).

Meanwhile, the anterior-posterior position information is established by a Nodal morphogen gradient secreted from the margin, inducing endoderm and mesoderm formation. It is the ratio of Nodal to BMP that leads to the differentiation of cells, not the total amount of mRNA (Fauny, Thisse, and Thisse 2009). The same principle applies to the ratio of Smad2 and Smad5, which can direct downstream Nodal and BMP signaling. Smad2 and Smad5 can selectively inhibit each other, creating a diverse environment in which cells respond (Soh, Pomreinke, and Müller 2020). However, the significance of the mutual antagonism between Nodal and BMP signaling remains unclear.

RNAscope, the higher-resolution smFISH method, allows the detection of lower gene expression levels (Gross-Thebing, Paksa, and Raz 2014). Individual mRNA spots can be classified into nascent mRNA, which is brighter and more prominent in the nucleus, and mature mRNA, most of which are in the cytoplasm and smaller. By the threshold of spot intensity or watershed method, mRNA segmentations are well used to quantify single cells or tissues (Mueller et al. 2013)(Carine Stapel et al., 2016). However, there are still a few issues remaining: first, how to distinguish mRNA spots from background or nonspecific binding; second, how to ensure that each mRNA spot represents only one individual mRNA since some mRNA might be close to each other, incredibly high-level expressed genes; third, how to distinguish

between nascent and mature mRNA; and fourth, to elucidate the spatial noise, 3D mRNA segmentation in whole-mount zebrafish embryos is required.

Here, we observed staggered expression between *szl* and *chd* in the marginal region of zebrafish gastrula embryos. Applying a high-resolution mRNA detection method to the input of mathematical modeling, we showed that Szl maintained BMP signaling with a production region shaped by Nodal signaling. We investigated the intrinsic noise by comparing the variability among nascent mRNAs; we revealed that BMP morphogen with high intrinsic noise are in the margin, suggesting that stochastic noise may be involved in DV patterning, achieved by varying the cell fate.

Materials And Methods

Zebrafish

Wide-type (TL) embryos and Tg(HA: GFP) fish were collected in E3 water and fixed at the desired stages.

smFISH using RNAscope method on cryosections

Zebrafish embryos were fixed with 4% PFA/PBS for 24 hours at 4°C. The embryos were washed with PBSTween and then dechorionated with forceps. Equilibrate the embryos into sucrose solutions: rinse first in 20% sucrose/PBS until all the embryos sink into the bottom, followed by 30% sucrose/PBS wash, wait until the embryos sink into the bottom. Then, the embryos were transferred into fresh 30% sucrose at 4°C. Embed embryos: Embed the embryos into Tissue-Tek® O.C.T. Forceps were used to orient the embryo to ensure that all the animal regions of the embryos faced the same direction. Blocks were quickly frozen in precooled isopentane on dry ice and stored at –80°C until cryosectioning. Ten-micrometer sections were attached to *Superfrost* Plus microscope slides. Keep the slides at -80°C for at most two weeks. Samples were subjected to the protocol (Catalog Number 320293) from RNAscope-based signal amplification (Advanced Cell Diagnostics). Samples were treated with Pretreat 2 and Pretreat 4 to further enhance the accessibility of probes. Mixed target probe hybridization was performed for 2 hours at 40°C. Four signal amplification systems then followed samples. DAPI was used at the last step to stain the nucleus, and the cells were mounted with Fluoromount-G (SouthernBiotech, Cat NO 0100-01).

smFISH using RNAscope method on whole-mount embryos

We used the protocol shown in our published paper(Li et al. 2020). Detailed probe information and dilutions are shown in Table 3. Make sure the embryos are in white, not yellow, color when air-dried from methanol.

RNA staining using RNAscope followed by pSmad staining

We tested different staining methods: 1) mRNA staining first, then pSmad immunostaining; 2) pSmad staining first, followed by mRNA staining. Test results showed that the first method was best. We made some modifications to the RNAscope staining section: the RNA probe concentration was two times the

original concentration, as shown in Table 1, and the RNA probe hybridization time was 12 hours. After mRNA staining, embryos were penetrated in 0.1% Triton X-100 in PBS for 1 hour at RT. Embryos were blocked in blocking buffer (4% BSA (Millipore Sigma, #126615), 1% DMSO, 0.1% Triton X-100 in PBS) overnight at 4°C and then stained with anti-phosphoSmad1/5/8 antibody (Cell Signaling Technology, #9511) at a 1:100 dilution in blocking buffer overnight at 4°C. Then, embryos were detected by goat anti-rabbit cross-adsorbed Alexa Fluor 647-conjugated antibody at a 1:500 dilution with DAPI overnight at 4°C (Thermo Fisher Scientific, #A21244).

Membrane labeling

Vybrant™ DiI Cell-Labeling Solution (Thermo Fisher, #V22885) was first injected into zebrafish embryos at one cell stage.

Bmp2b-Venus mRNA injection

The Venus-Bmp2b fusion protein was synthesized by the same method as in a previous paper (Zinski et al., 2017). Venus probe staining was performed by injecting 100 pg *venus-bmp2b* mRNA into one-cell stage embryos, and the embryos were fixed at 3 hpf.

Transcription inhibition

Inject 2 nl of 0.2 mg/ml alpha-amanitin (Sigma, #A2263) into the yolk at 4.5hpf. At the same time, 2 nl MQ water was injected into the yolk of the control groups. Fix all the embryos at 6 hpf according to the developmental stage of the control group.

Chemical Inhibitions

The BMP signaling inhibitor LDN193189 (Sigma, #SML0559), Nodal signaling inhibitor SB-505124 (Sigma, #S4696), and GSK inhibitor, also known as Wnt signaling activator BIO (Sigma, #B1686), were dissolved in DMSO to 10 mM as stock solutions and diluted in E3 medium at 50 μM, 50 μM, and five μM.

Image Acquisition

Embryos were mounted in 1% low melting agarose on 35 mm glass-bottom microwell dishes (Matek, P35G-1.5-10-C). Whole-mounted embryos were imaged with a 20×/1.0 Plan-Apochromat water immersion lens (D = 0.17 M27 75 mm) of Zeiss 800. *chd* mRNA was imaged by excitation at 555 nm wavelength. *bmp2b*, *tld*, and *szl* mRNA were imaged by excitation at 647 nm. The z interval is set to 3 μm, which is smaller than the pinhole thickness. Cryosections were imaged with a 63x oil objective of Zeiss 800.

Absolute Quantitative Digital PCR in whole embryos

Ten zebrafish embryos were collected at 6 hpf, dechorionated by placing in 1 mg/ml pronase, immersed and ground in TRIzol, and precipitated by isopropanol and chloroform. Eight microliters of HA-*bmp2b* mRNA synthesized from the pCS2(+)-HA-bmp2b plasmid(Little and Mullins 2009) was purified under the same conditions as the embryo group. RT reactions were performed in raw or purified HA-*bmp2b* mRNA and purified embryo mRNA using iScript™ Reverse Transcription Supermix (Bio–Rad, # 1708840),

followed by digital PCR with TaqMan hydrolysis probes using the QX100TM Droplet Digital PCR System. Primers against the *bmp2b* open reading frame across the intron region were as follows: forward primer (Tm: 60.5): 5'-CCA GCA GAG CAA ACA CGA TA-3', reverse primer (Tm: 59.9): 5'- CAT CTC CGA GAA CTT GGT CC-3'. The hydrolysis probe (Tm: 64.8) is located between the amplicon: 5'-CTC CGC TGC GGA GCT GCG CA-3'. Template cDNA was diluted to the dynamic range of QX100 (from 1 to 120,000 copies/20 µl reaction), as shown in step 3 of Table 1. mRNA numbers from raw and purified HA-*bmp2b* mRNA digital PCR results were used to calculate the loss of mRNA, and the RNA recovery rate was 26.81%. We quantified the bmp2b mRNA number in one embryo by the equation shown in step 4 of Table 1.

Individual cytoplasmic mRNA and nascent mRNA segmentation process

Image processing can be fulfilled by the five major steps shown in Table 2:

1. Drop-off correction on whole-mount embryos
2. Images convolution and filtering
3. mRNA spots segmentation by 2D or 3D connection
4. Big mRNA spots separation by 3D maximum detection
5. Nascent mRNA identification

Drop-off correction on whole-mount embryos

Embryos were imaged with an upright objective in the same orientation with the marginal region facing the bottom, making signal intensity reduced from the animal pole to the margin of embryos, as light is scattered when signal detection deepens into the lower layer of the embryo. We assumed that the nuclear intensity was consistent on average in Tg(HA-GFP) zebrafish. We collected and fixed zebrafish embryos at 8 hpf, followed by immunostaining using an anti-GFP antibody (Thermo Fisher, # A-11122) at a 1:500 dilution. The second antibody was the same channel used for *bmp2b* mRNA staining. Nucleus intensity in each layer of z-stacks was collected by the wavelet nucleus segmentation method in our lab(Wu et al. 2020) and averaged to represent the intensity in the z-direction. We used a linear equation to correct reduced-intensity: I_corrected= I_origin- z_position*dropoff_scale, in which dropoff_scale was -0.18 for 647 channels in 400 µm thick whole-mount embryos (n=5).

Images convolution and filtering

Intensity-corrected images were convolved with a Laplacian Gaussian filter (LOG) of size 15 with a standard deviation of 1.5. The only varied parameter was the threshold for the smallest intensity in whole processing, and the yielding number was compared with digital PCR data. The z-stack interval (3 µm) is smaller than the pinhole thickness (15.9 µm) on the objective of our confocal microscope, making each mRNA spot imaged more than once at the same XY position during consecutive slices. To obtain a remarkable mRNA total number, 3D mRNA segmentation in whole-mount embryos is indispensable.

mRNA spots segmentation by 2D or 3D connection

We implemented two methods to identify mRNA spots of whole-mount embryos.

1. 2D mRNA segmentation. Potential particles were identified as 2D connected masks in each slice using the MATLAB function bwlabel. The 2D matrix was transformed to a 3D matrix with the z position, which can be used to quantify the intensity of mRNA spots approximately five times faster than 3D mRNA segmentation. However, mRNA number will be overquantified in embryos.
2. 3D mRNA segmentation. 2D matrixes from each slice were first combined into a 3D matrix with the z position. We identified the connected mask at the 3D level using the MATLAB function bwconncomp. The 3D mask and number of all the mRNA spots were saved for the next step.

Big mRNA spots separation by 3D maximum detection

Cytoplasmic individual mRNAs can connect to one large spot. Potential large spots were first extracted if the spot intensity and pixel volume were larger than 1.5 times the average value. We find the 3D local maximums, including location and maximum intensity in the surrounding area of spots, by the MATLAB function nonMaxSupr of Piotr's toolbox, in which we set the radius to 2 pixels based on the averaged pixel volume.

Nascent mRNA identification

Nucleus segmentation was performed by the wavelet method. Nascent mRNA candidates were first selected if the spot intensity and pixel volume were larger than 1.5 times the average value; meanwhile, nascent mRNAs located inside the nucleus were identified by the nucleus and mRNA masks. The maximum number of nascent mRNAs in each nucleus was 4. Some cytoplasmic mRNA may still transit in the nucleus with a smaller size and intensity.

mRNA distribution visualization

To visualize the overall mRNA distribution throughout the embryo. Individual embryo mRNA data were mapped to a standard shape of a partial sphere depending on the specific developmental stages (4.7 hpf as 40% epiboly, 5.7 hpf as 50% epiboly). The embryo was then rotated to the DV axis based on the distribution of Chd mRNA (located at the dorsal most). Average distributed sample point clouds were created through the sphere; the accumulated mRNA intensity was collected at each sample point based on a defined circle area around this point. Multiple mRNA distributions from the same developmental stage were then averaged to obtain a general distribution map of the mRNA of individual species.

Ethics approval

All procedures on zebrafish adults and embryos were approved by the Purdue University Institutional Animal Care and Use Committee (IACUC: 1501001180A004)).

All procedures were performed in compliance with the ARRIVE guidelines.

All methods were performed in accordance with the relevant guidelines and regulations.

Code availability

smFISH segmentation and visualization codes have been deposited to GitHub: https://github.com/wang2594/smFISH-3D-quantification

Results And Discussion

Spatial detection of smFISH and protein at the single-cell level in whole-mount zebrafish embryos

To determine the relationship between input for secretion to the distributions of BMP signaling and BMP signaling activity, we used the RNAScope method to simultaneously detect multiple individual mRNAs at the cellular level in whole-mount embryos. *bmp2b* mRNA began to be expressed at the zygotic stage, showing an obvious gradient pattern of higher expression levels in the ventral region, whereas *chd* mRNA was expressed in the dorsal region at 5.7 hpf (Fig. 1A-C). *bmp2b* mRNA was detected at 2.5 hpf, with no *bmp2b* mRNA probe binding or background present, as a negative control (Fig. S1H-I). For the positive control, we injected *venus-bmp2b* fusion mRNA into zebrafish embryos at the one-cell stage, followed by *bmp2b* and *venus* mRNA staining at 3 hpf, when few endogenous *bmp2b* mRNAs were expressed. Based on observations, *bmp2b* mRNA colocalized well with *Venus* mRNA (Fig. S1 A-F). *szl*, as the target of BMP signaling, was also expressed in the ventral region (Fig. 1F-H). Nascent mRNA was observed exclusively in the nucleus and typically appeared as two or four large spots reflecting transcription activity, whereas mature mRNA appeared both inside and outside of the nucleus with smaller sizes, as shown in the diagram of Fig. 1J. We observed mature and nascent mRNA in whole-mount zebrafish embryos for the first time (Fig. 1D, E, I). *chd* nascent mRNA was easy to discern (Fig. 1E) compared with *bmp2b* and *szl* mRNA, the active loci of which were challenging to recognize, suggesting that nascent mRNAs are more evident during higher transcriptional activity. Furthermore, we used *tld* mRNA as a positive control to detect nascent mRNA. *tld* nascent mRNA was apparent in the EVL layer. When injected with α-amanitin, an inhibitor of RNA polymerase II and III, embryos only showed few mature *tld* mRNAs (Fig. S2E-F) compared to embryos injected with DMSO at 4.5 hpf (Fig. S2C-D). However, it was difficult to recognize the nascent mRNA of *bmp2b* by 2D imaging (Fig. S3A-B), prompting us to analyze bmp2b mRNA at the 3D level. Images were acquired using an upright confocal microscope with a 20x high NA (1.0) objective, which shows similar resolution to images taken on widefield microscopes (Fig. S1J, K).

Transcriptional responses to BMP signaling are mediated through pSmad. Comparison of BMP ligand levels with pSmad levels provides insight into positional information in this pathway. Comparison of pSmad levels with BMP target gene levels provides a measurement of transcriptional efficiency. Here, we demonstrated that we could detect pSmad and *bmp2b* (Fig. 1K, K') or szl (Fig. 1L, L') mRNA in identical embryos without sacrificing the intensity of each. Cell membrane staining is critical for single-cell level detection of mRNA and protein because of its importance for image segmentation. Unfortunately, the RNA scope protocol complicates this, as F-actin structures of cell membranes are broken up during preparation. Remarkably, we found that injecting membrane-labeling dye into zebrafish embryos at the one-cell stage circumvented this issue and provided membrane staining (Fig. 1M). Overall, we

demonstrate the viability of staining single molecular mRNA and protein and cell membranes at the single-cell level; this method will enable the investigation of positional information and study the relationship between transcription factors and target genes and noise at the cellular or embryonic level.

Absolute quantification of nascent and mature mRNA transcripts in whole-mount zebrafish embryos

Previously, mRNA quantification in zebrafish embryos was performed by observing the mRNA quantity on 2D segmentation on cryosections (Carine Stapel et al. 2016). This approach loses the overall shape of individual mRNAs of relatively large size. Some large spots, such as nascent mRNA and mature mRNA, can appear on different slices of whole embryos during imaging, influencing each spot's total intensity and volume matrix pixels. We developed 3D mRNA segmentation methods in whole-mount embryos following the flow chart shown in Table 2, during which intensity drop-off correction is a prerequisite (Fig. S3 A-D). Transcription is mainly maintained in the interphase. Up to 4 transcriptional loci can appear in the nucleus during DNA replication (Fig. 4F). This is consistent with similar findings in the mRNA segmentation of Drosophila embryos(Little, Tikhonov, and Gregor 2013) but was not observed in the 2D mRNA segmentation of zebrafish(Carine Stapel et al. 2016). To determine the individual mRNA candidates, we compared the *bmp2b* mRNA counts in entire embryos at 5.7 hpf by image quantification to those from digital PCR (table 1). Representative transcriptional loci are shown in Fig. 2A, B, with two large nascent mRNA spots inside of the nucleus. In digital PCR, the *bmp2b* mRNA probe targeted the middle of the *bmp2b* coding sequence. mRNA intensity is higher in mRNA strings transcribed by more than half and vice versa, so, on average, the intensity of an individual nascent mRNA can be estimated as half of the averaged intensity of mature mRNA to match the digital PCR results. Regardless of size and intensity, mature mRNAs were counted as one individual mRNA except for connected mature mRNAs, separated by local maximum (Fig. 2C). The only variable, the intensity threshold, can be determined by fitting a curve from individual mRNA numbers by different thresholds (Fig. 2D), coupled with a digital PCR number (table 1, n=273778). We found that the ratio of the maximum to the averaged value, including the volume matrix pixels (40/20) and intensity (10/5) of individual mRNAs, was approximately 2 (Fig. S3 G, H), which was also found in previous work(Raj et al. 2008). Many individual mRNAs with a smaller area and lower intensity were also considered the actual single mRNA molecule shown in the peak of Fig. S3 G, H. Combining mRNA segmentation and digital PCR in whole embryos, the background signal was authentically removed from smFISH images. Nascent and mature mRNA was divided based on location, size, and intensity.

Determining critical factors in quantifying mRNA distribution across whole embryos

To detect the relationship between mRNA number and intensity at different positions on whole embryos, we established a whole sphere mesh to represent the zebrafish embryos at the blastula stage and mapped the mRNA spots to the corresponding mesh. Interestingly, the total mRNA number and intensity were linear with each other at each mesh (Fig. 2E). The *bmp2b* mRNA 3D distributions across whole

embryos were also similar between different mRNA numbers (Fig. 2G) and mRNA intensities (Fig. 2H) in each mesh, being more highly expressed in the ventral animal and marginal regions. Embryos were rotated into standard alignment using *chd* mRNA expression (Fig. 2I) as a marker of the dorsal region. Notably, the mRNA number in each mesh was sensitive to the intensity threshold in mRNA segmentation (Fig. 2F). All of these results suggest that the most accurate and efficient way to visualize the smFISH distribution is to first determine the intensity threshold by combining 3D mRNA segmentation and digital PCR and then apply this threshold to 2D mRNA segmentation of more samples, which is approximately five times faster than 3D mRNA segmentation. Using the intensity from 2D mRNA segmentation, we effectively quantified averaged *bmp2b* (Fig. S3 E, F) and *szl* mRNA (Fig. 3E) distributions in more embryos. *bmp2b* mRNA production evolved from occurring highly in the ventral animal region at 4.7 hpf (Fig. S3 E) to occurring highly in both the ventral animal and ventral marginal regions at 5.7 hpf (Fig. S3 F), suggesting that *bmp2b* starts to play a vital role in the margin between 4.7 hpf and 5.7 hpf.

Szl maintains the inhibition level in the marginal layer by BMP and Nodal signaling.

Higher-precision methods will give us a better resolution to detect the mRNA spatial distribution appropriate for mathematical modeling input. We found that *bmp2b* showed a gradient from ventral to dorsal in the ventral marginal and animal regions (Fig. 3D, Fig. S3 E). *chd*, as the target of Nodal signaling(Bradham et al. 2010), was expressed in the margin at 5.7 hpf (Fig. 3F) and disappeared in the margin at 8 hpf (Fig. S4 C,C'), which is consistent with Nodal expression from the blastula to gastrula stage(Rogers et al. 2017). Interestingly, *szl*, as the target of BMP signaling, was only expressed on the animal excluded from the ventral margin (Fig. 3E) and not colocalized with pSmad in the margin when simultaneously detecting *szl* and pSmad in whole-mount embryos at 5.7 hpf (Fig. S4 B, B'). Remarkably, *szl* recovered the expression in the margin at the gastrula stage (Fig. S4 C, C'). This finding is consistent with another BMP target gene, foxi1, induced by high levels of BMP and low Nodal levels (Soh, Pomreinke, and Müller 2020). We postulated that *szl* might be inhibited by Nodal, which is only expressed in the marginal layer at 5.7 hpf. To test this hypothesis, we utilized a Nodal inhibitor (SB-505124) and a BMP signaling inhibitor (LDN193189) to evaluate the role of Nodal and BMP signals on *szl* expression. Importantly, we found that application of the nodal inhibitor led to resumed expression of *szl* at the ventral margin (Fig. 3A, A', B, B'), and *szl* was entirely blocked by the BMP inhibitor (Fig. 3C, C'). These results suggest that BMP and Nodal cooperatively shape the expression of *szl*.

Previous work shows that BMP and Nodal signaling can selectively inhibit each other to specify the cell type(Soh, Pomreinke, and Müller 2020). Our data implied that this mutual inhibition might play an essential role in BMP morphogen maintenance. To determine the impact of different *szl* expression on a three-dimensional level, we modified our previously built three-dimensional growing domain model, which includes the growth of epiboly and 3D patterning(Li et al. 2020); the mathematical equations for this model are shown in Table 4. We adopted 182 sets of parameters screened from our 10 million 1D simulations(Tuazon et al. 2020) and applied different expression regions of *szl* as simulation input, with margin (Fig. 3G) or excluded from the margin (Fig. 3H). We calculated the NRMSD of modeling output data and experimental pSmad data, representing the fitting error, on the margin with two different *szl*

expression inputs. Strikingly, some of the NRMSD could be significantly reduced by removing *szl* expression in the margin (Fig. 3I) and were closely related to the ratio of the *szl* production rate to ki, representing the strength of Szl protein suppression (Fig. 3J). These results suggest that *szl* and *chd* change the expression region in the margin where dorsal-ventral patterning is determined to maintain the inhibition level of BMP morphogen.

BMP morphogen intrinsic noise implies the cell state

Understanding the stochastic nature of the signaling response between different cells is a fundamental challenge in biology. Intrinsic noise mainly comes from elements involved in transcription rates and can be evaluated by two-factor assays (Elowitz et al. 2002) or the sizes of transcribing loci (Stapel, Zechner, and Vastenhouw 2017)(Little, Tikhonov, and Gregor 2013). Extrinsic noise originates from the differences among cells, such as cell cycle stage or differential abundance of transcription factors (Zopf et al., 2013). We can detect intrinsic noise through the volume pixels and intensity of nascent mRNA by 3D mRNA segmentation. We observed nascent mRNA in 49% of all nuclei ranging from 1 to 4 loci (Fig. 4F), implying that approximately half of the cells are in interphase. Strikingly, we observed four nascent mRNAs in the form of 2 pairs of sister chromatids, indicating DNA undergoing replication. Of the observed nuclei, 20% had only one nascent mRNA (Fig. 4E, F), suggesting that the transcriptional activity is independent between two chromosomes. This could also happen when more than one nascent mRNA colocalizes with each other. To assess the instantaneous transcriptional activity of the BMP morphogen, we evaluated the variation among the total intensity of each nascent mRNA in the nuclei. Importantly, we found that the intrinsic noise was much higher in the marginal region for nuclei with both (Fig. 4A, B) and four nascent mRNAs (Fig. 4C, D). In a whole-mount embryo, the nascent mRNA expression region was similar to the *bmp2b* mRNA in a whole-mount embryo (Fig. 3D), and only the marginal region was highly noisy, which is clearly shown in the amplified figures (Fig. 4B, 4D). Representative nascent mRNAs with higher noise levels are shown in Figure 4E and were compared with those with lower noise levels (Fig. 2B). Zebrafish embryos start to establish DV patterning in the margin at 5.7 hpf, where and when a consistent noisy pattern is observed for intrinsic BMP morphogen noise, noise can represent the state of the cell across whole embryos.

Declarations

Ethics approval

All procedures on zebrafish adults and embryos were approved by the Purdue University Institutional Animal Care and Use Committee (IACUC: 1501001180A004)).

All procedures were performed in compliance with the ARRIVE guidelines.

All methods were performed in accordance with the relevant guidelines and regulations.

Code availability

smFISH segmentation and visualization codes have been deposited to GitHub: https://github.com/wang2594/smFISH-3D-quantification

ACKNOWLEDGEMENTS

We thank Aasakiran Madamanchi for proofreading the paper.

Competing INTERESTS

None

Funding

This work was supported by the National Institutes of Health [R01HD073156].

References

1. Bier, E. & De Robertis, E. M. 2015. “BMP Gradients: A Paradigm for Morphogen-Mediated Developmental Patterning.” *Science*348(6242)
2. Bradham, C. A. *et al.* 2010.“Urchin Embryos.”328(2):221–33
3. Briscoe, J. & Stephen Small Morphogen Rules: Design Principles of Gradient-Mediated Embryo Patterning.. ” *Development (Cambridge)*, **142** (23), 3996–4009 (2015).. &#8220
4. Carine Stapel, L. *et al.* Automated Detection and Quantification of Single RNAs at Cellular Resolution in Zebrafish Embryos.. ” *Development (Cambridge)*, **143** (3), 530–39 (2016).. &#8220
5. Elowitz, M. B. *et al.* Stochastic Gene Expression in a Single Cell.. ”, **297** (5584), 1183–86 (2002).. &#8220
6. Fauny, J., Daniel, B. T. & Christine Thisse The Entire Zebrafish Blastula-Gastrula Margin Acts as an Organizer Dependent on the Ratio of Nodal to BMP Activity.. ” *Development*, **136** (22), 3811–19 (2009).. &#8220
7. Gregor, T., Tank, D. W., Wieschaus, E. F. & William Bialek Probing the Limits to Positional Information.. ”, **130** (1), 153–64 (2007).. &#8220
8. Gross-Thebing, T. & Paksa, A. and Erez Raz. 2014. “Simultaneous High-Resolution Detection of Multiple Transcripts Combined with Localization of Proteins in Whole-Mount Embryos.” *BMC Biology* 12(1)
9. Hasty, J., Pradines, J., Dolnik, M. & Collins, J. J. Noise-Based Switches and Amplifiers Forgene Expression.. ” *Proceedings of the National Academy of Sciences of the United States of America*, **97** (5), 2075–80 (2000).. &#8220
10. Kærn, M., Elston, T. C., Blake, W. J. & James J. Collins Stochasticity in Gene Expression: From Theories to Phenotypes.. ” *Nat. Rev. Genet*, **6** (6), 451–64 (2005).. &#8220

11. Li, L., Wang, X., Mullins, M. C. & David M. Umulis Evaluation of BMP-Mediated Patterning in a 3D Mathematical Model of the Zebrafish Blastula Embryo.. " *Journal of Mathematical Biology*, **80** (1–2), 505–20 (2020).. &#8220
12. Little, S. C. & Mullins, M. C. Bone Morphogenetic Protein Heterodimers Assemble Heteromeric Type I Receptor Complexes to Pattern the Dorsoventral Axis.. " *Nat. Cell Biol*, **11** (5), 637–43 (2009).. &#8220
13. Little, S. C., Tikhonov, M. & Thomas Gregor Precise Developmental Gene Expression Arises from Globally Stochastic Transcriptional Activity.. ", **154** (4), 789–800 https://doi.org/10.1016/j.cell.2013.07.025. (2013).. &#8220
14. Mueller, F. *et al.* FISH-Quant: Automatic Counting of Transcripts in 3D FISH Images.. " *Nat. Methods*, **10** (4), 277–78 https://doi.org/10.1038/nmeth.2406. (2013).. &#8220
15. Oka, Y. & Sato, T. N. Whole-Mount Single Molecule FISH Method for Zebrafish Embryo.. " *Sci. Rep*, **5**, 1–8 (2015).. &#8220
16. Raj, A. *et al.* Imaging Individual MRNA Molecules Using Multiple Singly Labeled Probes.. " *Nat. Methods*, **5** (10), 877–79 (2008).. &#8220
17. Rogers, K. W. *et al.* Nodal Patterning without Lefty Inhibitory Feedback Is Functional but Fragile.. " *eLife*, **6**, 1–20 (2017).. &#8220
18. Soh, G., Huiming, A. P., Pomreinke & Müller, P. 2020. "Integration of Nodal and BMP Signaling by Mutual Signaling Effector Antagonism." *Cell Reports* 31(1)
19. Stapel, L., Carine, C., Zechner & Vastenhouw, N. L. Uniform Gene Expression in Embryos Is Achieved by Temporal Averaging of Transcription Noise.. " *Genes and Development*, **31** (16), 1635–40 (2017).. &#8220
20. Tuazon, F. B. *et al.* Article Proteolytic Restriction of Chordin Range Underlies BMP Gradient Formation Ll Ll Proteolytic Restriction of Chordin Range Underlies BMP Gradient Formation.. " *CellReports*, **32** (7), 108039 https://doi.org/10.1016/j.celrep.2020.108039. (2020).. &#8220
21. Wu, T. C. *et al.* 2020. "WaveletSEG: Automatic Wavelet-Based 3D Nuclei Segmentation and Analysis for Multicellular Embryo Quantification." *bioRxiv*: 2020.07.24.220285
22. Zhang, L. *et al.* Noise Drives Sharpening of Gene Expression Boundaries in the Zebrafish Hindbrain.. " *Mol. Syst. Biol*, **8** (613), 1–12 (2012).. &#8220
23. Zinski, J. *et al.* Systems Biology Derived Source-Sink Mechanism of Bmp Gradient Formation.. " *eLife*, **6(**, e22199 (2017).. &#8220
24. Zopf, C. J., Quinn, K., Zeidman, J. & Narendra Maheshri Cell-Cycle Dependence of Transcription Dominates Noise in Gene Expression.. " *PLoS Computational Biology*, **9** (7), 1–12 (2013).. &#8220

Tables

Due to technical limitations, table 1 to 4 is only available as a download in the Supplemental Files section.

Figures

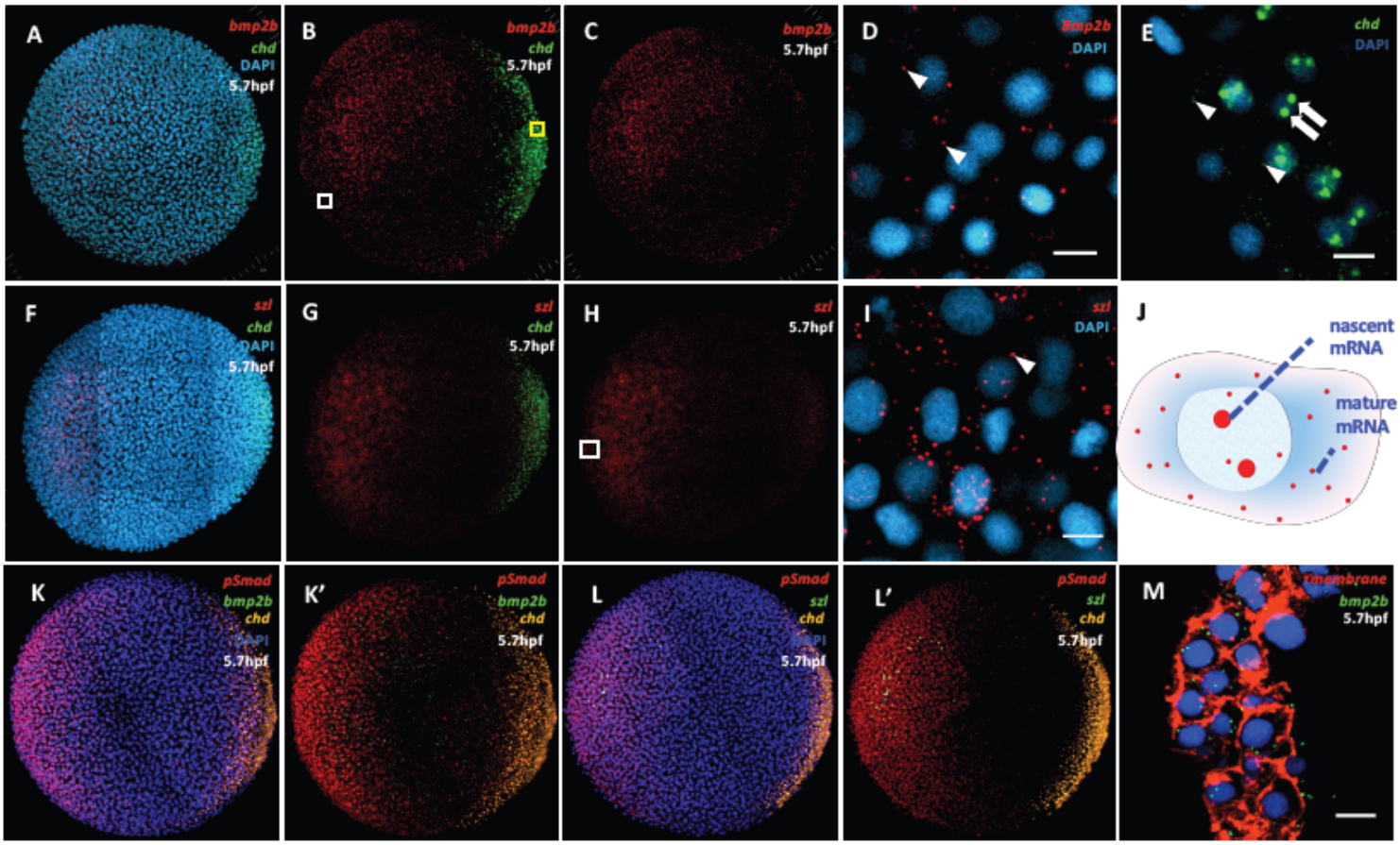

Figure 1

Specific detection of mature and nascent mRNA in zebrafish whole-mount embryos with the RNAscope method. (A-E) bmp2b (red) and chd (green) single molecular mRNA expression imaged from animal view at 5.7hpf, with nucleus stained by DAPI (blue). (B) bmp2b and chd in A. (C) bmp2b in A. (D) White box in B at higher magnification. Arrowhead: bmp2b mature mRNA. Scale bar: 10 μm. (E) The yellow box in B at higher magnification. Arrowhead: chd mature mRNA; Arrow: chd nascent mRNA. Scale bar:10 μm. (F-I) szl (red) and chd (green) single molecular mRNA expression imaged from animal view at 5.7hpf, and nucleus are stained by DAPI (blue). (G) szl and chd in F. (H) szl in F. (I) White box in H at higher magnification. Arrowhead: szl mature mRNA. Scale bar: 10 μm. (J) example of nascent and mature mRNA. (K-L') Simultaneous expression of pSmad (red) and bmp2b (K, K') or szl (L, L') (green) single molecular mRNA at 5.7 hpf, with nuclei stained by DAPI (blue). (M) Membrane labeling (red) when detecting bmp2b mRNA (green) at 5.7 hpf. Scale bar:10 μm.

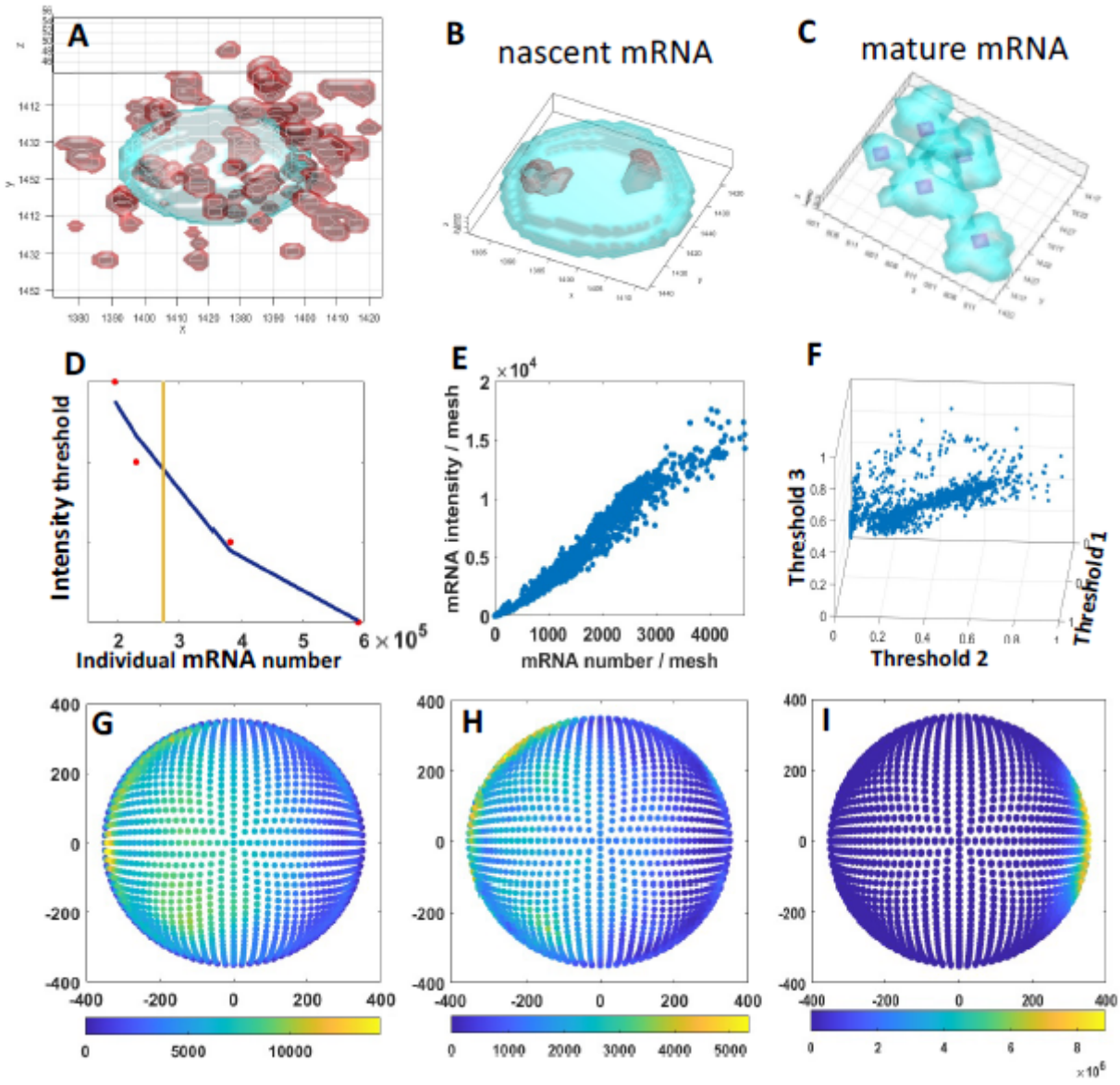

Figure 2

Quantification of bmp2b nascent and mature mRNA in whole mount embryos at 5.7 hpf. (A-C) mRNA and nuclear segmentation with nuclear mask (light blue) and smFISH masks (red). (B)Nascent mRNA from (A). (C) Separation of connected cytoplasmic mature mRNA from (A). Purple dots indicate the local maximum of single cytoplasmic mRNA. (D) Individual mRNA number after entire image processing of a single embryo with different intensity thresholds. Scatter red dots represent the test value with blue linear fitting. The yellow line shows the individual mRNA number from digital PCR. (E) mRNA number and intensity scatter plot of whole-mount embryos. (F) mRNA number scatter plot at three intensity thresholds in whole-mount embryos. (G)bmp2b mRNA number distribution. (H) bmp2b mRNA intensity distribution. (I) chd mRNA intensity distribution.

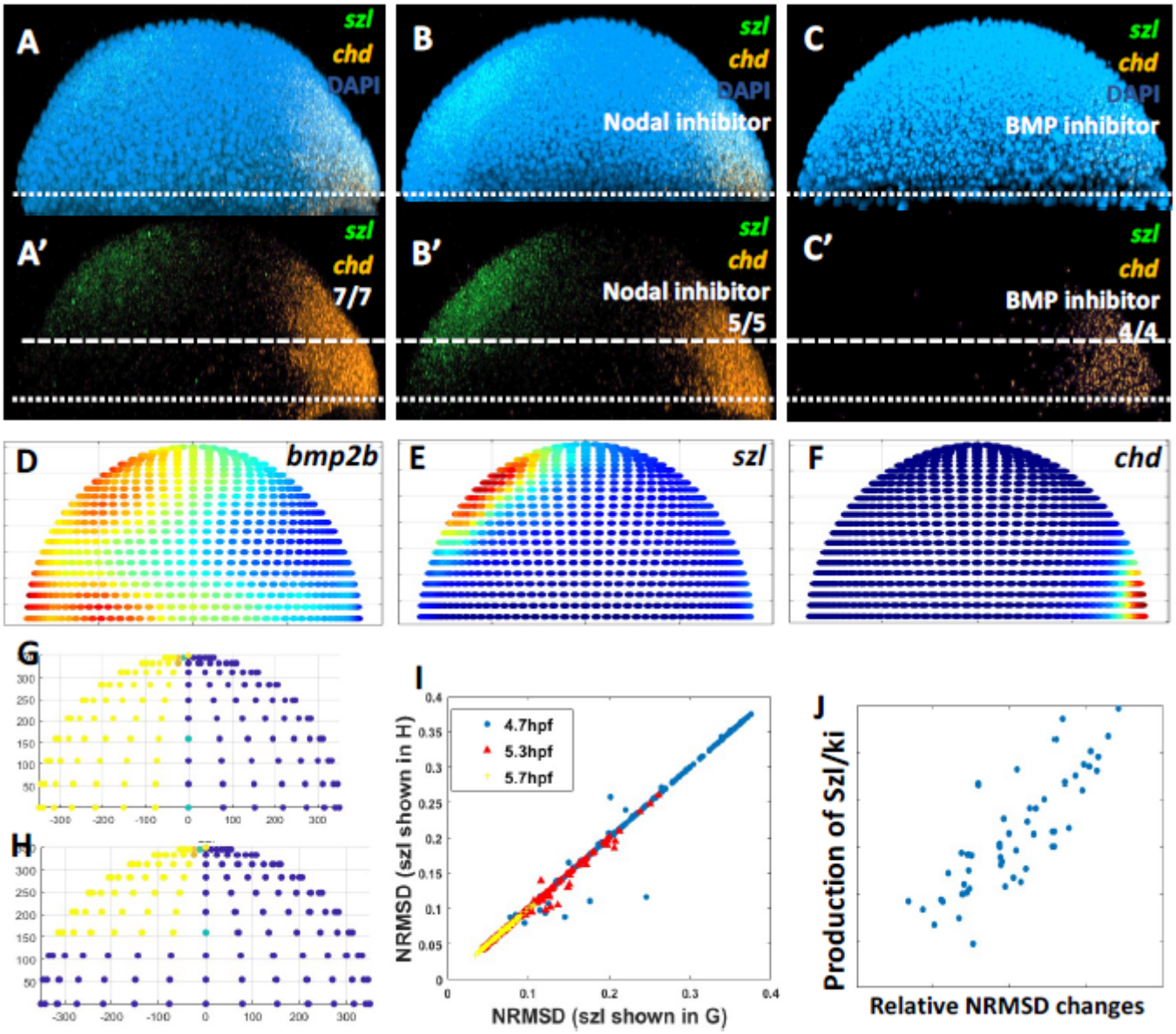

Figure 3

Szl mRNA expression maintains the BMP morphogen gradient by BMP and Nodal signaling. (A-C') szl (green) and chd (orange) single molecular mRNA expression imaged from lateral view at 5.7 hpf, with nuclei stained by DAPI (blue). (A, A') WT control. (B, B') Nodal inhibitor. (C, C') BMP inhibitor. (D-F) Averaged mRNA intensity distribution from the lateral view at 5.7 hpf. (D)bmp2b, n=4. (E)szl, n=7 (F) chd, n=7. (G-H) szl input in 3D mathematical modeling. (I) Scatter plot of NRMSD from different szl inputs in G and H. (J) Scatter plot of RNMSD and the ratio of szl production to ki.

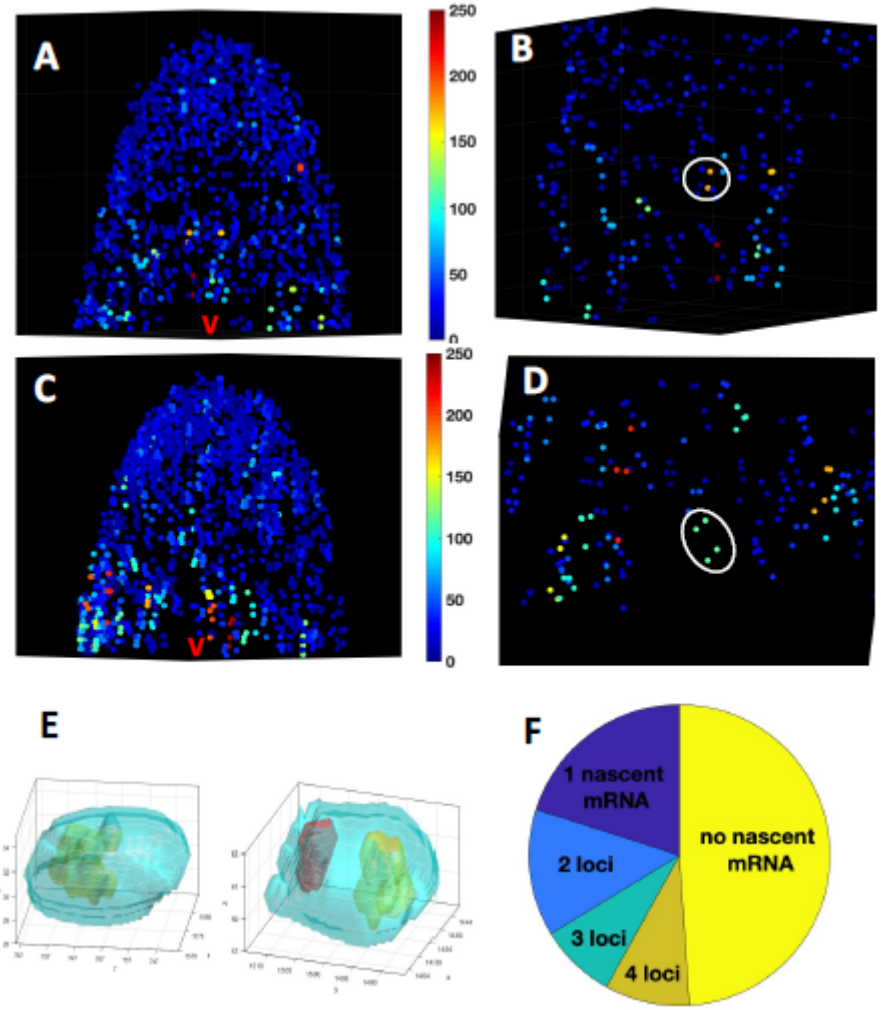

Figure 4

bmp2b Intrinsic noise indicating the cell state across the whole embryo at 5.7 hpf. (A) Intrinsic noise distribution of the nucleus with two nascent mRNAs. The lateral view and ventral is in the middle. (B) Higher magnification from A. Two representative nascent mRNAs are marked with circles. (C) Intrinsic noise distribution of the nucleus with four nascent mRNAs. The lateral view and ventral is in the middle. (D) Higher magnification from C. Representative 4 nascent mRNAs in one nucleus are marked with circles. (E) Representative image of one nascent mRNA in the nucleus and two nascent mRNAs in the nucleus of different sizes. (F) Statistics of nucleus number with different nascent mRNA numbers.

Supplementary Files

This is a list of supplementary files associated with this preprint. Click to download.

- table1.png
- table2.png
- table3.png

- table4.png
- SupFigures.pdf
- SupFiglegend.docx